ELSEVIER

Nuclear Instruments and Methods in Physics Research A 433 (1999) 240–246

NUCLEAR INSTRUMENTS & METHODS IN PHYSICS RESEARCH Section A

www.elsevier.nl/locate/nima

Reconstruction algorithms in the Super-Kamiokande large water Cherenkov detector

On behalf of Super-Kamiokande collaboration

M. Shiozawa[a,b]

[a]*Institute for Cosmic Ray Research, University of Tokyo, Tanashi, Tokyo 188-8502, Japan*
[b]*Kamioka Observatory, Higashi-Mozumi, Kamioka-cho, Yoshiki-gun, Gifu-ken, 506-1205 Japan*

Abstract

The Super-Kamiokande experiment, using a large underground water Cherenkov detector, has started its operation since first April, 1996. One of the main physics goals of this experiment is to measure the atmospheric neutrinos. Proton decay search is also an important topic. For these analyses, all measurement of physical quantities of an event such as vertex position, the number of Cherenkov rings, momentum, particle type and the number of decay electrons, is automatically performed by reconstruction algorithms. We attain enough quality of the analyses using these algorithms and several impressive results have been addressed.

PACS: 29.40.K

Keywords: Atmospheric neutrinos; Proton decays; Super-Kamiokande

1. Introduction

The Super-Kamiokande experiment, which utilizes a large water Cherenkov detector, has rich physics topics such as atmospheric neutrinos, solar neutrinos, proton decays, and so on. Thanks to the huge target volume of 22.5 kton and the large photo coverage area, this detector has a capability to collect neutrino events with high statistics and to perform the precise measurement of physical quantities. Recently, the Super-Kamiokande collaboration reported the evidence of neutrino oscillation in the atmospheric neutrino observation [1–4]. These exciting results were also reported in this workshop [5]. Moreover, baryon number violated proton decays, which are predicted by Grand Unified Theories, have been searched for and we set the most stringent limit on the partial lifetime of the proton [6].

In the atmospheric neutrino and proton decay analyses, we measure the physical quantities of an event such as vertex position, the number of Cherenkov rings, momentum, particle type and the number of decay electrons. We start from the vertex fitter program to obtain the vertex position of events. With the knowledge of the vertex position, the ring fitter positively identifies each ring. After

* Tel.: + 81-578-5-9611; fax: + 81-578-5-2121.
E-mail address: masato@icrr.u-tokyo.ac.jp (M. Shiozawa)

0168-9002/99/$ - see front matter
PII: S0168-9002(99)00359-9

that, the particle identification program identifies the particle type for each ring. For single ring events, this particle-type information is used to improve the reconstructed vertex position. Finally, the momentum for each ring is determined and decay electrons are identified. The vertex fitter, ring fitter, particle identification, and momentum reconstruction are described here. Moreover, ring separation, which separates the observed photoelectrons (p.e.'s) in each photomultiplier tube (PMT) and assigns the fractional p.e.'s to each Cherenkov ring, is explained for the reconstruction of multi-ring events.

2. Super-Kamiokande detector

The Super-Kamiokande detector is a large water Cherenkov detector which is located deep underground to reduce cosmic ray muon backgrounds. The detector is a cylindrical stainless-steel tank holding 50 kton of ultra-pure water. The detector is optically separated into two concentric cylindrical regions, the inner detector and outer detector.

The inner detector measuring 36.2 m height and 33.8 m in diameter is viewed by 11146, inward-facing, 50 cm diameter PMTs. These PMTs uniformly surround the inner detector region giving 40% photocathode coverage. The data acquisition system records the number and arrival times of the photons collected in each PMT. From these values, along with the positions of the PMTs, the events are reconstructed.

The outer detector completely surrounds the inner detector region with 2.0–2.2 m thickness. 1885 outward pointing 20 cm PMTs view this region and entering cosmic ray muons are rejected by the outer detector information.

3. Vertex fitter

The reconstruction procedure starts from the vertex fitting. The principle of the fitting is that the timing residual ((photon arrival time)-(time of flight)) distribution should be most peaked with the correct vertex position. In Fig. 1, the time-of-flight (TOF) subtracted TDC distributions are shown

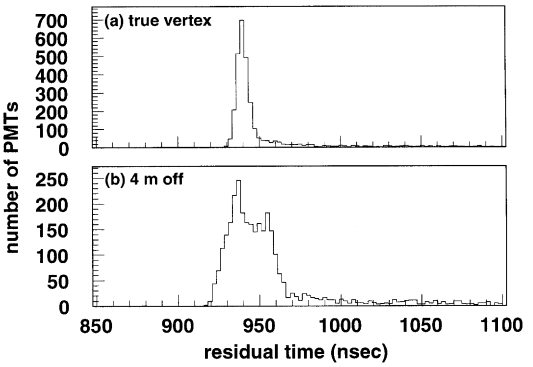

Fig. 1. The residual time distributions after TOF subtraction. The time of flight is calculated with (a) true vertex position and (b) 4 m off from the true vertex position. With the true vertex, the residual time distribution has a sharp peak.

with (a) true vertex position and (b) wrong position 4 m off from the true vertex position. With the true vertex, the residual time distribution has a sharp peak as shown in Fig. 1(a). The finite width of the distribution comes from the time resolution of the PMTs. The long tail is made by scattered light and reflected light from the detector wall. On the other hand, with the wrong vertex position, the residual time becomes a wide distribution as shown in Fig. 1(b).

To find the vertex position where the timing residual distribution becomes most peaked, the fitting estimator G is defined as

$$G = \sum_i \frac{1}{\sigma_i^2} \exp\left(- \frac{(t'_i - t_0)^2}{2(\langle\sigma\rangle \times 1.5)^2} \right) \quad (1)$$

where i is a PMT number, σ_i is timing resolution of the ith PMT as a function of detected p.e.'s, $\langle\sigma\rangle$ is the timing resolution for the detected p.e.'s averaged over fired PMTs and t'_i is the TOF subtracted timing information of the ith PMT. In the TOF subtraction, the track length of the charged particle is taken into account. The vertex fitter searches for a vertex position where the estimator G takes maximum value.

The performance of the vertex fitter is investigated for the proton decay mode of $p \to e^+\pi^0$. Using Monte Carlo events, the vertex resolution is estimated to be 18 cm. The vertex resolution for single ring events are 34 and 25 cm for electrons

and muons, respectively, for the momentum region of $p < 1.33\,\mathrm{GeV}/c$. These performances are obtained after vertex position correction using determined particle types.

4. Ring fitter

After reconstruction of the vertex position, possible rings are looked for and probable rings are reconstructed in this ring fitter. Using the reconstructed ring(s), we can reconstruct the total momentum and total invariant mass of $p \to e^+\pi^0$ events and those of atmospheric neutrino events. We use a known technique for a pattern recognition, Hough transformation [7], to search for possible ring candidates. The essence of the Hough transformation is shown in Fig. 2. Suppose there are four fired PMTs on the unknown ring (radius r) and we want to find the center of the ring (left figure). By Hough transformation, the detected p.e.'s are mapped to a circle with radius r centered on the PMT. All mapped circles cross at the center of the unknown ring. By accumulating the mapped circles, we can find the peak in the Hough space, giving the center of the unknown ring.

Before the mapping, the p.e. contribution from the rings which already have been regarded as true rings are subtracted in order to enhance the possible ring candidates. In the ring fitter, the Hough space is made up of two-dimensional arrays divided by polar angle Θ (36 bins) and azimuthal angle Φ (72 bins), resulting in 36×72 pixels. These angles are measured from the reconstructed vertex. Detected p.e.'s in each fired PMT, which are corrected for acceptance and attenuation length, are mapped to pixels (Θ_i, Φ_i) for which the opening angle toward the PMT is 42°. In the actual case, a Cherenkov ring in the Super-Kamiokande detector has a broad p.e. distribution rather than an ideal thin circle. In order to take into account the actual p.e. distribution, the expected p.e. distribution for a $500\,\mathrm{MeV}/c$ electron as a function of opening angle θ is used as a weight in the p.e.'s mapping. Namely, the corrected p.e.'s of a fired PMT are mapped to pixels (Θ_i, Φ_i), for which the opening angles toward the PMT are θ, with weight of expected p.e.'s $Q_e(\theta)$.

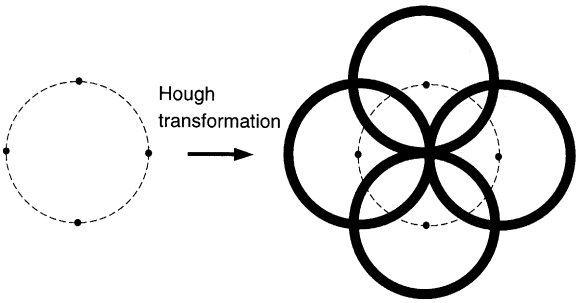

Fig. 2. The Hough transformation. Suppose there are four fired PMTs on the unknown ring (radius r) and we want to find the center of the ring (left figure). By Hough transformation, the detected p.e.'s are mapped to a circle with radius r centered on the PMT (right figure). By accumulating the mapped circles, we can find the peak in the Hough space, giving the center of the unknown ring.

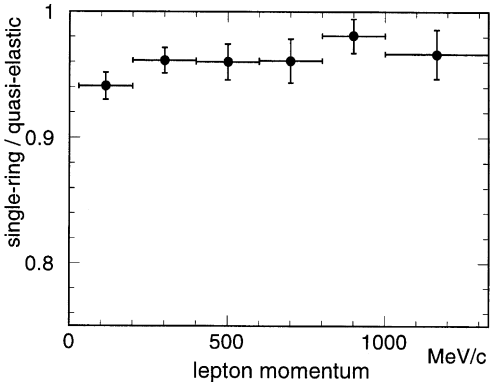

Fig. 3. The efficiency of single-ring identification for quasi-elastic scattering events. Using the atmospheric neutrino Monte Carlo, the fraction of (single-ring quasi-elastic events)/(quasi-elastic events) is plotted as a function of momentum. The efficiency is $\sim 96\%$ for the momentum region shown.

Peaks found in the Hough space are identified as centers of possible ring candidates. However, any ring candidate for which the direction is very close to one of the true ring directions (opening angle $< 15°$) is discarded as a fake candidate made by the true ring. For the $p \to e^+\pi^0$ events, 98% of the events are reconstructed as two or three rings. The two-ring classification is primarily for events with one of the two γ rings taking only a small fraction of the π^0's energy or overlapping too much with other rings. The performance of the ring fitter for single-ring events is also studied. Fig. 3 shows

the efficiency of single-ring identification for quasi-elastic scattering events of atmospheric neutrinos. The efficiency is $\sim 96\%$ for the momentum region of $p < 1.33$ GeV/c.

5. Particle identification

The particle identification (PID) classifies a particle as a showering particle ($e^{\pm}$,γ) or a nonshowering particle ($\mu^{\pm}$, $\pi^{\pm}$), using the photon distribution of its Cherenkov ring. Showering (nonshowering) particles are sometimes called e-like (μ-like). At first, the expected p.e. distributions are calculated with an assumption of the particle type. Using the expected p.e. distributions, the following likelihood is calculated for the electron and muon assumptions.

$$L(\mathrm{e\ or\ }\mu) = \prod_{\theta_i < (1.5 \times \theta^c)} \mathrm{prob}(q_i, q_i^{\mathrm{exp}}(\mathrm{e}) \text{ or } q_i^{\mathrm{exp}}(\mu)). \quad (2)$$

Here L(e) is calculated using the electron expectation q_i^{exp}(e) and L(μ) is calculated using the muon expectation $q_i^{\mathrm{exp}}(\mu)$. prob(q_i, q_i^{exp}) is the statistical probability of observing q_i with the expectation of q_i^{exp} and defined as

$$\mathrm{prob}(q^{\mathrm{obs}}, q^{\mathrm{exp}}) = \begin{cases} \dfrac{1}{\sqrt{2\pi}\sigma} \exp\left(-\dfrac{(q^{\mathrm{obs}} - q^{\mathrm{exp}})^2}{2\sigma^2} \right) & \text{for } q^{\mathrm{obs}} > 20 \text{ p.e.} \\ \text{convolution of one p.e.} & \text{for } q^{\mathrm{obs}} < 20 \text{ p.e.} \\ \text{distribution and Poisson} & \\ \text{distribution} & \end{cases} \quad (3)$$

where the σ is defined as $\sigma^2 = (1.2 \times \sqrt{q^{\mathrm{exp}}})^2 + (0.1 \times q^{\mathrm{exp}})^2$ in which the factor 1.2 takes into account the difference of the actual PMT resolution from the ideal one and the factor 0.1 corresponds to the uncertainty of the gain calibration. The probability function for $q^{\mathrm{obs}} < 20$ p.e. is calculated by convolution of the measured one p.e. distribution and a Poisson distribution. The production of the probability in Eq. (2) is performed for all of the ith PMTs for which the opening angles toward the ring direction θ_i are within 1.5 times the Cherenkov opening angle. Optimizations of q_i^{exp}(e) and q_i^{exp}(μ) are performed by changing the direction and the Cherenkov opening angle of the ring in order to get maximum-likelihood values of L(e) and L(μ).

In order to combine the likelihood with another estimator which uses the Cherenkov opening angle, the likelihood is transformed into the χ^2 distribution as

$$\chi^2(\mathrm{e\ or\ }\mu) = \frac{1}{\log_{10} \mathrm{e}} \times (-\log_{10} L(\mathrm{e\ or\ }\mu)) - \text{constant}. \quad (4)$$

Using the χ^2(e) and χ^2(μ), probabilities from the Cherenkov ring pattern are calculated as

$$P^{\mathrm{pattern}}(\mathrm{e\ or\ }\mu) = \exp\left(-\frac{1}{2}\left(\frac{\chi^2(\mathrm{e\ or\ }\mu) - \chi^2_{\mathrm{min}}}{\sigma_{\chi^2}} \right)^2 \right) \quad (5)$$

where $\chi^2_{\mathrm{min}} = \min[\chi^2(\mathrm{e}), \chi^2(\mu)]$ and σ_{χ^2} is calculated from the degree of freedom as $\sigma_{\chi^2} = \sqrt{2N_{\mathrm{D}}}$ where N_{D} is the number of PMTs used in Eq. (2).

Moreover, another probability is defined using only the Cherenkov opening angle. Given the reconstructed opening angle as $\theta^c \pm \delta\theta$, the probability is calculated as

$$P^{\mathrm{angle}}(\mathrm{e\ or\ }\mu) = \text{constant} \times \exp\left(-\frac{1}{2}\left(\frac{\theta^c - \theta^{\mathrm{exp}}(\mathrm{e\ or\ }\mu)}{\delta\theta} \right)^2 \right) \quad (6)$$

where θ^{exp}(e) and θ^{exp}(μ) is the expected Cherenkov opening angle for an electron and muon, respectively, calculated from estimated ring momentum using the detected p.e.'s. Using the probability from the pattern and the probability from the angle, total probability is defined as

$$P(\mathrm{e\ or\ }\mu) = P^{\mathrm{pattern}}(\mathrm{e\ or\ }\mu) + P^{\mathrm{angle}}(\mathrm{e\ or\ }\mu). \quad (7)$$

For a single ring event, when P(e) > P(μ) (P(e) < P(μ)), the ring is identified as showering (nonshowering) type. However, for a multi-ring event like a $p \to e^+\pi^0$, we do not use the angle probability P^{angle} in the particle-type determination. That is because a γ from the decay of the

π^0 sometimes penetrates in water (mean free path of ~ 55 cm) before causing the electromagnetic shower and this gives a small reconstructed opening angle of the Cherenkov ring. The small opening angle makes $P^{\text{angle}}(\text{e})$ small, resulting in small $P(\text{e})$. Therefore, for the multi-ring event, we use only the pattern probability $P^{\text{pattern}}(\text{e})$ and $P^{\text{pattern}}(\mu)$ to determine the particle type. Namely, when $P^{\text{pattern}}(\text{e}) > P^{\text{pattern}}(\mu)$($P^{\text{pattern}}(\text{e}) < P^{\text{pattern}}(\mu)$), the ring is identified as showering (nonshowering) type.

The performance of the PID is important for the $p \to e^+\pi^0$ search to detect signal but reject background events. This is also essential for the atmospheric neutrino observation. For single ring events, the particle misidentification probability is estimated to be less than 1.0% using the atmospheric neutrino Monte Carlo. This is confirmed with stopping cosmic ray muons and their associated decay electrons. The PID performance was also checked using a 1 kton water Cherenkov detector with e and μ beams from the 12 GeV proton synchrotron at KEK [8]. However, the misidentification probability differs between single and multi-ring events due to overlapping rings. Using the $p \to e^+\pi^0$ Monte Carlo sample the multi-ring misidentification is estimated to be 2%.

6. Ring separation

The "ring separation" program determines the fraction of p.e.'s in each PMT due to each ring. As a result, this separation gives the observed p.e. distributions for individual rings. We need this separation for the ring fitting and the particle identification of each ring as well as the momentum reconstruction. The strategy of the separation is as follows. Given a vertex position and each ring direction, the expected p.e. distribution for each ring as a function of opening angle θ is calculated according to the observed p.e. distribution assuming the flat distribution in azimuthal angle ϕ. Using the expected p.e. distribution $q_{i,n}^{\text{exp}}$, where i refers to a PMT number and n refers to a ring number, the observed p.e.'s of the ith PMT (q_i) are separated as

$$q_{i,n} = q_i \times \frac{q_{i,n}^{\text{exp}}}{\sum_{n'} q_{i,n'}^{\text{exp}}} \tag{8}$$

where $q_{i,n}$ is the fractional p.e.'s of the ith PMT assigned to the nth ring. With the assumption of the ϕ symmetry, the $q_{i,n}^{\text{exp}}$ can be calculated from $Q_n^{\text{exp}}(\theta_{i,n})$ which is the expected p.e. distribution as a function of opening angle θ. Therefore, calculation of the $Q_n^{\text{exp}}(\theta)$ is essential in the ring separation.

At first step, all $q_{i,n}^{\text{exp}}$ are set assuming that all particles are electrons. Then, initial expected p.e. distributions are determined by minimizing the following χ^2:

$$\chi_n^2 = \sum_{\theta_{i',n} < 70^\circ} \left(\frac{q_{i'} - \sum_{n'} q_{i',n'}^{\text{exp}}}{\sqrt{q_{i'}}} \right)^2 . \tag{9}$$

The summation is performed for all of i'th PMT for which the opening angle toward the nth ring direction $\theta_{i',n}$ is within 70°. By minimizing the χ^2's, we obtain the initial separated p.e.'s $q_{i,n}$ using the converged $q_{i,n}^{\text{exp}}$ and Eq. (8).

Using the initial separated p.e.'s $q_{i,n}$, we make the expected p.e. distribution $Q_n^{\text{exp}}(\theta)$ as a function of the opening angle θ toward the nth ring direction. The $Q_n^{\text{exp}}(\theta)$ is the expected p.e.'s projected on a hypothetical spherical surface centered at the reconstructed vertex. For making the $Q_n^{\text{exp}}(\theta)$ from the $q_{i,n}$, we need to correct the number of p.e.'s for the distance from the vertex, the attenuation length, and acceptance. By summing up the corrected p.e.'s within each opening angle bin, we obtain the $Q_n^{\text{exp}}(\theta)$. Here, optimization is done so that main contribution to the $Q_n^{\text{exp}}(\theta)$ comes from non-overlapping region of the ring. Proper normalization and smoothing are also done in making the $Q_n^{\text{exp}}(\theta)$.

In the next step, we iteratively optimize the $Q_n^{\text{exp}}(\theta)$ using the likelihood function. The expected p.e.'s for ith PMT $q_{i,n}^{\text{exp}}$ is recalculated from the $Q_n^{\text{exp}}(\theta_{i,n})$. Using the new $q_{i,n}^{\text{exp}}$, separation of the observed p.e.'s is performed again by maximizing the following likelihood function L_n:

$$L_n = \sum_{\theta_{i',n} < 70^\circ} \log\left(\text{prob}(q_{i'}, \sum_{n'} \alpha_{n'} \cdot q_{i',n'}^{\text{exp}}) \right) \times \sqrt{Q_n^{\text{exp}}(\theta_{i',n})} \times \min[1, \sqrt{\theta_n^{\text{c}}/\theta_{i',n}}] \tag{10}$$

where $\alpha_{n'}$ is a parameter used for the optimization, θ_n^{c} is the reconstructed Cherenkov opening angle of

the nth ring, and the $prob(q_{i',n'}, \sum_{n'}\alpha_{n'} \cdot q^{exp}_{i',n'})$ is the probability of observing $q_{i'}$ with expected p.e.'s of $\sum_{n'}\alpha_{n'} \cdot q^{exp}_{i',n'}$ and defined in Eq. (3). The factor $\sqrt{Q^{exp}_n(\theta_{i',n})}$ and $\min[1, \sqrt{\theta^c_n/\theta_{i',n}}]$ in the Eq. (10) enhance the contributions from PMTs around the Cherenkov edge and inside of the Cherenkov edge, respectively. By optimizing the factor α_n, the program looks for the best α_n which maximizes the likelihood function L_n. At first, α_1 is optimized so that L_1 is maximized. The same optimization is iteratively performed for the second ring, third ring, and so on until all α_n's converge.

Given the best α_n's, the observed p.e.'s of the ith PMT are separated again as

$$q_{i,n} = q_i \times \frac{\alpha_n \cdot q^{exp}_{i,n}}{\sum_{n'}\alpha_{n'} \cdot q^{exp}_{i,n'}}. \quad (11)$$

Finally, the procedure from making Q^{exp}_n to Eq. (11) is repeated two more times (three times in total), to improve the separated p.e.'s $q_{i,n}$. An example of the result of the ring separation is shown in Fig. 4. In the figures, observed p.e.'s in a three ring event of $p \to e^+\pi^0$ are separated and assigned to one of the rings. We can see the clearly separated ring.

7. Momentum determination

The momentum is estimated from the total sum of p.e.'s detected within a 70° half opening angle from the reconstructed ring direction. The number of p.e.'s collected in each PMT is corrected for light attenuation in water, PMT angular acceptance, and PMT coverage. In the momentum reconstruction, we assume that showering particles are electrons and nonshowering particles are muons. For single-ring events, the reconstructed momentum resolution is estimated to be $\pm(2.5/\sqrt{E(\mathrm{GeV})} + 0.5)\%$ for electrons and $\pm 3\%$ for muons. For multi-ring events, the ring separation program (Section 6) is applied with particle-type assumption to determine the fraction of p.e.'s in each PMT due to each ring. Then, the momentum for each ring is determined by the same method used for single-ring events. The reconstructed momentum resolution is $\pm 10\%$ for each ring in the $p \to e^+\pi^0$ events.

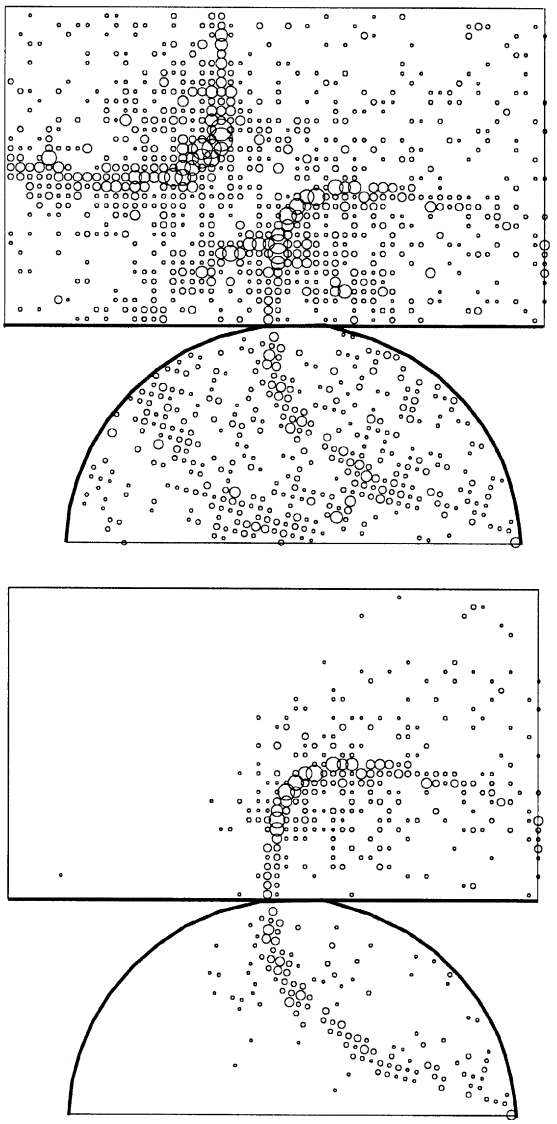

Fig. 4. An example of the result of the ring separation. PMTs which are located in the part of the detector and have more than one p.e. are shown. The top figure shows a $p \to e^+\pi^0$ Monte Carlo event in which three Cherenkov rings are seen. The observed p.e.'s in each PMT are separated by "ring separation". The separated p.e.'s for the right ring are shown in the bottom figure. The observed p.e.'s are clearly separated and assigned to the ring.

The energy scale stability is checked by the reconstructed mean energy of decay electrons from stopping cosmic ray muons. It varies within $\pm 1\%$ over the exposure period. The absolute energy scale

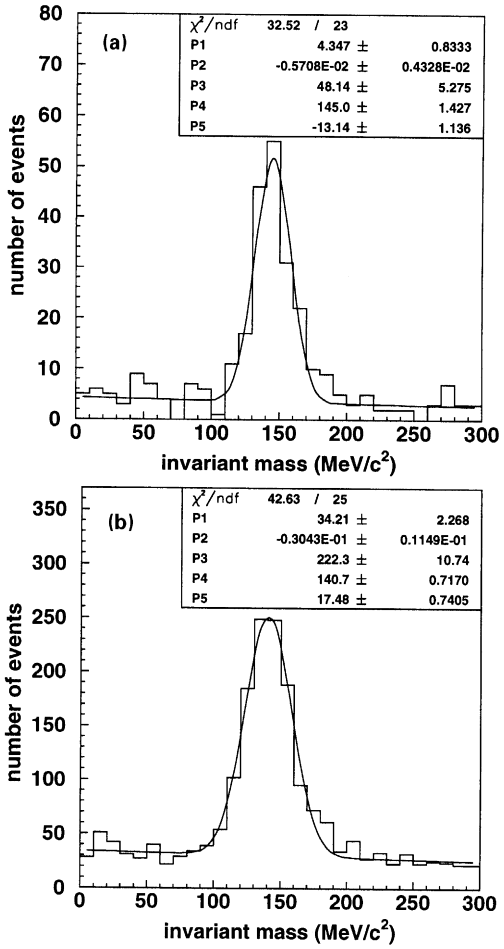

Fig. 5. The invariant mass distributions for neutrino-induced π^0 events. (a) Data and (b) atmospheric neutrino Monte Carlo. Reconstructed mass distributions are fitted by a combined function of $f(x) = P1 + P2 \times x + P3 \times \exp[-(x - P4)^2/2P5^2]$. The fitted peaks of invariant mass agree well with each other within 3%.

is checked with many calibration sources such as electrons from a linear accelerator [9], decay electrons from stopping cosmic ray muons, stopping cosmic ray muons themselves, and the reconstructed mass of π^0 events observed in atmospheric neutrino interactions. Fig. 5 shows the reconstructed mass of π_0 events in (a) data and (b) atmospheric neutrino Monte Carlo. From comparisons of these sources and Monte Carlo simulation, the absolute calibration error is estimated to be smaller than $\pm$ 3%.

8. Summary

The reconstruction algorithms for the atmospheric neutrino observation and proton decay search by the Super-Kamiokande detector have been described. The vertex resolution is 18 cm for $p \to e^+\pi^0$ events and 34 and 25 cm for single-ring electrons and muons, respectively, for the momentum region of $p < 1.33\,\mathrm{GeV}/c$. In ring fitting, 98% of the $p \to e^+\pi^0$ events are reconstructed as two or three rings and 96% of quasi-elastic scattering events of atmospheric neutrinos are reconstructed as single ring events. The misidentification probability of particle types is only of order 1%. The energy resolution is estimated as $\sim$ 3% and systematic uncertainty of the energy scale is $\pm$ 3%.

Acknowledgements

We gratefully acknowledge the cooperation of the Kamioka Mining and Smelting Company. The Super-Kamiokande experiment was built from, and has been operated with, funding by the Japanese Ministry of Education, Science, Sports and Culture, and the United States Department of Energy.

References

[1] Y. Fukuda et al., Phys. Lett. B 433 (1998) 9.
[2] Y. Fukuda et al., Phys. Lett. B 436 (1998) 33.
[3] Y. Fukuda et al., Phys. Rev. Lett. 81 (1998) 1562.
[4] T. Kajita, talk given at International Conference on Neutrino Physics and Astrophysics, Takayama, 1998.
[5] M. Shiozawa, talk given at International Workshop on Ring Imaging Cherenkov Detectors, Dead-Sea, 1998.
[6] M. Shiozawa et al., Phys. Rev. Lett. 81 (1998) 3319.
[7] Davies, E. Roy, Machine Vision: Theory, Algorithms, Practicalities, Academic Press, San Diego, 1997.
[8] S. Kasuga et al., Phys. Lett. B 374 (1996) 238.
[9] M. Nakahata et al., Nucl. Instr. and Meth. A 421 (1999) 113.